


RESEARCH ARTICLE

Homography-based uncalibrated visual servoing with neural-network-assisted robust filtering scheme and adaptive servo gain

Jinlin Gu^{1,2} | Wenrui Wang^{1,2} | Ang Li^{1,2} | Mingchao Zhu^{1,2}  | Lihua Cao² | Zhenbang Xu^{1,2}

¹CAS Key Laboratory of On-orbit Manufacturing and Integration for Space Optics System, Changchun Institute of Optics, Fine Mechanics and Physics, Chinese Academy of Sciences, Changchun, China

²University of Chinese Academy of Sciences, Beijing, China

Correspondence

Mingchao Zhu, CAS Key Laboratory of On-orbit Manufacturing and Integration for Space Optics System, Changchun Institute of Optics, Fine Mechanics and Physics, Chinese Academy of Sciences, Changchun 130000, China.
Email: mingchaozhu@gmail.com

Funding information

Jilin Province and Chinese Academy of Sciences Cooperation in Science and Technology High-Tech Industrialization Special Funds Project, Grant/Award Number: 2018SYHZ0004; Jilin Scientific and Technological Development Program, Grant/Award Number: 2018020102GX; National Natural Science Foundation of China, Grant/Award Numbers: 11672290, 11972343

Abstract

In this paper, a homography-based uncalibrated visual servo system with neural-network-assisted robust filtering scheme and adaptive servo gain is presented. This system employs a homography-based task function which is robust to image defects. A neural-network-assisted robust filtering method which combines the new form of smooth variable structure filter (SVSF) with a radial basis function (RBF) neural network is proposed to estimate the total Jacobian between task function and robot joints. The RBF neural network in this filtering method plays the role as a corrector to further improve the accuracy and compensate the interference caused by the measurement errors of image features. The controller that directly controls the robot joints based on the estimated total Jacobian is designed for achieving the robustness to robot parameters errors. By adopting this filtering scheme, the visual servo system shows better accuracy and convincing anti-interference ability. In addition, a novel Q-learning strategy is introduced for this homography-based system to make adaptive adjustment for the servo gain. This adaptive gain enables the system to achieve a faster convergence speed while ensuring the accuracy. Several simulations and experiments have been carried out to verify the performance of the proposed system.

KEYWORDS

neural network, projective homography, Q-learning, robust filtering scheme, uncalibrated visual servo

1 | INTRODUCTION

Visual servo control is a servo control method that realizes the precise positioning of robot's end-effector or camera by employing visual feedback. It can replace manpower to perform automatic operations in harsh environments and has a wide range of applications in

many fields, such as unmanned aerial vehicles [1, 2], underwater vehicles [3, 4], and space robots [5, 6]. According to the different ways of employing visual feedback, visual servoing can be divided into position-based visual servoing (PBVS), image-based visual servoing (IBVS), and hybrid visual servoing. PBVS obtains the information of relative pose in 3D Cartesian space based

on visual feedback and forms a closed loop-system [7, 8]. IBVS directly uses 2D visual feedback to construct the controller and constitutes a closed-loop system [9–12]. Hybrid visual servoing combines the above two categories, so it is also called 2.5D visual servoing [13]. Among these methods, IBVS has attracted more attention in recent years due to its better accuracy and robustness [14].

In IBVS strategies, the pixel coordinates of image feature points are usually directly connected in series to form the task function. The most pressing of issues in IBVS is to obtain the mapping relationship from robot to 2D image plane, which is defined as the image Jacobian matrix. In traditional method, the parameters of image Jacobian matrix are obtained by system calibration and depth estimation [15]. However, the performance of these methods highly depends on the accuracy of system calibration. Calibration errors and parameter changes will cause a serious impact on the performance of the system. To solve this problem, image-based uncalibrated visual servoing (IBUVS) based on online techniques have been proposed and widely used [16–20]. In this strategy, image Jacobian matrix is estimated online in each control period to construct the controller without calibrating the system in advance. Therefore, IBUVS has better accuracy and shows robustness to calibration errors and parameter changes.

In practical applications, IBUVS encounters some bottlenecks as well. Image feature defects caused by motion blur, inconspicuous background contrast, and occlusion of the field of view are the main reasons for servo failure. Uncalibrated visual servoing based on projective homography (PHUVS) is the latest proposed solution that can overcome image feature defects [21, 22]. In the PHUVS method, a target with more image feature points is adopted, and the elements of the homography matrix between the current and the desired image features are used to construct the task function. The homography matrix can be calculated as long as there are no less than four pairs of matched feature points. Therefore, even if partial image feature defects occur, servo process will not be interrupted. It is worth noting that no matter how many feature points are identified, the dimension of the task function remains constant. In Gu et al. [23], the dimension of homography-based task function is further reduced.

Another major issue is the online estimation of image Jacobian matrix. There are two points should be considered here. The first is the modeling uncertainty caused by this local and linear approximation of the nonlinear and highly coupled mapping relationship between task function and robot. The other is the influence of the measurement noises caused by

measurement errors of image features. Classic image Jacobian identification methods such as Broyden-based method [24] and exponentially weighted recursive least square update method [25] are not convincing in dealing with unknown system structure and noise interference. Particle filter demonstrates its anti-interference ability, but its performance is unstable and its process is complicated [26]. In recent years, the Kalman filter (KF) which works as an optimal state estimator for ideal linear dynamic systems with Gaussian white noise, has become the mainstream method and show better accuracy [19, 21, 22]. However, in most practices, the measurement noises cause by the measurement errors of image features are not always Gaussian white noise, and its statistical characteristics are more complicated. In this case, the KF will degenerate into a sub-optimal filter and its accuracy will decrease or even diverge [27]. Except for unstable Sage–Husa adaptive KF method, adaptive KF methods based on fuzzy logic are proposed to handle the noise with unknown statistical characteristics [28, 29]. However, their performances depend on the formulation of fuzzy rules, and these methods are mainly aimed at unknown Gaussian white noise. These limitations lead to insufficient applicability and stability. In a recently proposed variational Bayesian (VB) adaptive KF method, the noise covariance matrices are inferred based on the VB approach. However, it mainly solves the problem of unclear statistical characteristics of Gaussian white noise, and the improvement of accuracy is based on more iterations [30].

Combining the KF method with neural networks (NNs) or other filter method is another feasible idea. In Shenshu and Zhaoying [31], a feed-forward NN plays the role of filtering gain for reducing the noise interference. In Vaidehi et al. [32], a back-propagation NN is incorporated into KF method to improve the accuracy of tracking the maneuvering targets by correcting the modeling error. A multilayered NN is used to reduce the nonlinear modeling error in tracking Kalman filter (TKF) in Takaba et al. [33]. It is worth noting that these KF-NN methods still rely on “known” noise statistics or an accurate linear state space model of system. In Zhong et al. [27], NN is introduced into KF method to compensate the interference of noise without the above limitations and have a convincing performance. However, this method requires a large input dimension, resulting in a huge structure and heavy computational burden of NN. In previous works [23, 34, 35], a new form of the SVSF method (VBL-SVSF) is proposed, which introduces the concept of the state error covariance matrix of KF method into SVSF method to derive the optimal time-varying smoothing boundary layer (VBL). This derived smoothing boundary

layer can be regarded as a measurement of the interference caused by modeling uncertainty and measurement noise. By switching between the optimal VBL-based gain (or KF gain) and the conservative standard SVSF gain, the optimality as shown in the KF method can be pursued when the interference is not obvious; otherwise the conservative and robustness of the SVSF method will be sought. It shows convincing accuracy and anti-interference performance than the SVSF method and KF method. However, even if a certain degree of improvement can be obtained, the decrease in accuracy caused by measurement noise is still inevitable. Moreover, inappropriate filter parameters of the VBL-SVSF method will lead to decrease in accuracy as well.

Another problem which is often ignored is the selection of servo gain. When the initial error of system is large, a large servo gain will easily lead to the instability of the system, while a small servo gain will cause the system to converge too slowly. In recent years, the adaptive gain that takes both stability and convergence speed into account has attracted more attention. In Xu et al. [36], a monitor is designed to make a rough adjustment of servo gain, but its weak adaptive ability limits its performance and applicability. For nonlinear second-order system, Jin et al. [37] put forward an adaptive state-feedback-based method to adjust the gain. In Wang et al. [38], a finite-time observer is designed to estimate the error, and the gain is obtained based on the uncertainty of estimation error. However, the design of the state-feedback loop and observer is very complicated, making these methods unsuitable for visual servo. In comparison, Q-learning with self-learning ability is a more reasonable choice. In Shi et al. [39], the servo gain for a decoupled visual servo system is adjusted by Q-learning and shows strong adaptive ability to the environment. In Kang et al. [40], Q-learning is adopted to adaptively adjust the servo gain for an extreme learning machine-based visual servo system, and the convergence speed of this system is improved.

In this paper, a novel PHUVS system with NN-assisted robust filtering scheme and adaptive servo gain is proposed. In this system, a homography-based task function with robustness to image defects is adopted, and a discrete controller that directly controls robot joints based on estimated total Jacobian is designed for obtaining the robustness to robot parameter errors. Without various calibrations of system parameters, a novel robust filtering scheme which combines the VBL-SVSF method and RBF NN is presented to do online estimation of the total Jacobian matrix, which is the mapping relationship between the homography-based task function and the robot joints. In this novel filtering scheme, an RBF NN is integrated into the VBL-SVSF method as a

corrector of state estimation error, for further improving the robustness and compensating the estimation error caused by the measurement errors of image features. Compared with the KF method and VBL-SVSF method, our proposed scheme shows more convincing performance. Moreover, a novel Q-learning strategy corresponding to the proposed homography-based system is presented to obtain the Q-table for decision making. According to the convergent Q-table, the servo gain is adjusted adaptively at each interval to achieve the optimal value, for improving the convergence speed while ensuring the accuracy. Finally, the complete novel PHUVS framework employing NN-assisted robust filtering scheme and Q-learning are described. The results of simulations and experiments prove the improvement of the novel robust filtering scheme in the positioning accuracy and the anti-interference ability. The increase in convergence speed brought by the proposed Q-learning strategy has been verified as well.

The structure of this paper is introduced as follows. The basic principle of PHUVS is introduced in the next section. In Section 3, the NN-assisted robust filtering scheme is proposed. In Section 4, a method of adaptive gain using Q-learning is proposed. The complete framework of the proposed PHUVS is described in Section 5. Results of experiment and simulation are given to verify the effectiveness of the proposed system in Section 6. At last, the conclusion is presented in Section 7.

2 | VISUAL SERVOING BASED ON PROJECTIVE HOMOGRAPHY

The basic framework of PHUVS is introduced in this section. For eye-in-hand configuration system, the camera moves with the robot end-effector and the purpose of visual servoing can be understood as controlling the camera to reach the desired pose. The current coordinate system F and the desired coordinate system F^* of this eye-in-hand camera are defined as shown in Figure 1. $R \in \mathbb{R}^{3 \times 3}$ and $t \in \mathbb{R}^{3 \times 1}$ are the orientation matrix and displacement vector between F and F^* expressed in F . d^* is the distance between the desired projection center and the target plane π . $p_i = [u_i \ v_i \ 1]'$ and $p_i^* = [u_i^* \ v_i^* \ 1]'$ are the homogeneous pixel coordinates of the feature point P captured by the camera in current pose and the camera in desired pose, respectively. There is a mapping relationship between these two homogeneous coordinates as

$$p_i = \underbrace{Z_i^* K (R + t n^{*T}) K^{-1} p_i^*}_{H_{3 \times 3}}, \quad (1)$$

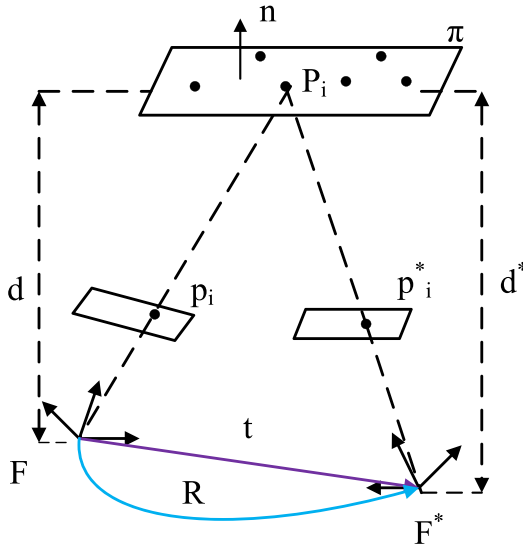


FIGURE 1 Projective homography model

where K is the internal parameter matrix of camera and n^* is the normal vector of π expressed in the F^* with length $\|n^*\| = 1/d^*$. Z_i and Z_i^* are the depth information of feature point P in F and F^* , respectively. H is defined as the projective homography matrix which can be estimated with at least four pairs of matched feature points. There is an unknown scale relationship between the estimated and the defined homography matrix as $\bar{H} = \beta H$, where β is independent of the depth ratio Z_i^*/Z_i . Since the homography matrix can be scaled with any scale, a constraint $\bar{h}_9 = 1$ is defined to obtain a unique solution in each period, where \bar{h}_9 is the last element of \bar{H} . Then, the homography-based task function is formed by the elements of the estimated homography matrix \bar{H} as

$$\bar{h} = [\bar{h}_1 \ \bar{h}_2 \ \dots \ \bar{h}_8]^T_{8 \times 1}. \quad (2)$$

Gu et al. [23] prove that if and only if \bar{H} is an identity matrix, the current camera pose coincides with the desired pose, which means $R=I$ and $t=0$. Thus, the error vector of system is denoted as

$$s = [\bar{h}_1 \ \bar{h}_2 \ \dots \ \bar{h}_8]^T - [1 \ 0 \ 0 \ 0 \ 1 \ 0 \ 0 \ 0]^T. \quad (3)$$

A proportional control law that controls the robot joints can be designed as

$$\dot{q} = -\lambda(J_r J_c)^+ s, \quad (4)$$

where J_c is the Jacobian matrix between task function and robot end-effector. J_r is the robot Jacobian and λ is the servo gain.

3 | NN-ASSISTED ROBUST FILTERING SCHEME FOR TOTAL JACOBIAN ESTIMATION

In uncalibrated visual servo system, analytical form of the hand-eye relationship J_c between task function and end-effector cannot be obtained. In addition, the calculation of the Jacobian J_r between robot joints and end-effector is sensitive to the robot parameter errors [23]. Therefore, a robust identification strategy combining the VBL-SVSF method and RBF NN is introduced to estimate the total Jacobian between task function and robot joints directly. The detail of this strategy is introduced in this section.

3.1 | State space model for total Jacobian estimation

The total Jacobian J_t which refers to the mapping relationship between the task function and the n degree of freedom (DOF) robot joints is defined as

$$\dot{\bar{h}} = J_t \dot{q}, \quad (5)$$

$$J_t = \begin{bmatrix} \partial \bar{h}_1 / \partial q_1 & \dots & \partial \bar{h}_1 / \partial q_n \\ \vdots & \ddots & \vdots \\ \partial \bar{h}_8 / \partial q_1 & \dots & \partial \bar{h}_8 / \partial q_n \end{bmatrix}_{8 \times n} = \begin{bmatrix} J_{11} & \dots & J_{1n} \\ \vdots & \ddots & \vdots \\ J_{81} & \dots & J_{8n} \end{bmatrix}_{8 \times n}, \quad (6)$$

where \dot{q} represents the joint velocities of an n -DOF robot. The total Jacobian can be estimated online by state space identification method. Thus, a linear discrete-time state space model of uncalibrated visual servo system is defined as follows:

$$X_{K+1} = A X_K, \quad (7)$$

$$Z_K = H_K X_K + \eta_K, \quad (8)$$

where η_k is defined as the measurement noise with a covariance matrix V_k . A is the state transition matrix of the system and it is an identity matrix. The state vector X_K is constructed by concatenating each row of the total Jacobian matrix as

$$X_K = [J_{11} J_{12} \cdots J_{8n}]_{8n \times 1}^T. \quad (9)$$

The observation vector Z_K is the amount of change in the task function between two adjacent sampling period as

$$Z_K = \bar{h}(K+1) - \bar{h}(K). \quad (10)$$

And the observation matrix H_K is constructed by joint velocities and sampling time ΔT as

$$H_K = \begin{bmatrix} \dot{q}^T \Delta T & \cdots & 0 \\ \vdots & \ddots & \vdots \\ 0 & \cdots & \dot{q}^T \Delta T \end{bmatrix}_{8 \times 8n}. \quad (11)$$

When the measurement noise η_k complies with the statistical characteristic of Gaussian white noise, the KF method can obtain the optimal estimation of system state vector X_K . In practice, the statistical characteristic of measurement noise caused by the measurement errors of image features is often more complex and unavailable. Coupled with the interferences caused by other modeling uncertainties, the accuracy of the KF method will decrease. In the VBL-SVSF method, by deriving time-varying boundary layer and switching the filter gains, the optimality as shown in the KF method can be pursued when these interferences are not obvious; otherwise the conservatism and robustness of the SVSF method will be sought. However, even if a certain degree of improvement can be obtained, the decrease in accuracy caused by measurement noise still cannot be ignored. In addition, the inappropriate switching threshold will lead to a decrease in accuracy as well. Thus, an NN-assisted VBL-SVSF scheme is proposed to further improve the performance of the VBL-SVSF method.

3.2 | NN-assisted filtering scheme

In the VBL-SVSF method, the concept of state error covariance matrix is introduced into the original SVSF method [34], which is defined as

$$P_k = \begin{bmatrix} \tilde{E}\{e_1^T e_1\} & \cdots & \tilde{E}\{e_1^T e_{8n}\} \\ \vdots & \ddots & \vdots \\ \tilde{E}\{e_{8n}^T e_1\} & \cdots & \tilde{E}\{e_{8n}^T e_{8n}\} \end{bmatrix}_{8n \times 8n}, \quad (12)$$

$$e_i = X_{Ki} - \hat{X}_{Ki}, \quad (13)$$

where $\tilde{E}\{e_i^T e_j\}$ represents the mean of $e_i^T e_j$. X_{Ki} and \hat{X}_{Ki} are the i th elements of the true state vector X_K and the estimated state vector \hat{X}_K , respectively. To minimize the diagonal elements of state error covariance matrix P_K , an optimal time-varying smoothing boundary layer Θ_{K+1} is derived as follows. The a priori state vector is updated according to the system model 7 at first:

$$\hat{X}_{K+1|K} = \hat{X}_{K|K}, \quad (14)$$

where $\hat{X}_{K|K}$ is the estimated state vector in previous iteration. Next, the a priori state error covariance matrix is obtained:

$$P_{K+1|K} = P_{K|K} + W_K, \quad (15)$$

where $P_{K|K}$ is the a posteriori state error covariance matrix in the previous iteration. Then, the residuals vectors of system are calculated as

$$e_{Z,K+1|K} = Z_{K+1} - H_{K+1} \hat{X}_{K+1|K}, \quad (16)$$

$$e_{Z,K|K} = Z_K - H_K \hat{X}_{K|K}. \quad (17)$$

And the optimal time-varying smoothing boundary layer Θ_{K+1} can be calculated as

$$\Upsilon_{K+1} = H_{K+1} P_{K+1|K} H_{K+1}^T + V_{K+1}, \quad (18)$$

$$E_{K+1} = \mu |e_{Z,K|K}|_{abs} + |e_{Z,K+1|K}|_{abs}, \quad (19)$$

$$\Theta_{K+1} = \left(\bar{E}_{K+1}^{-1} H_{K+1} P_{K+1|K} H_{K+1}^T \Upsilon_{K+1}^{-1} \right)^{-1}, \quad (20)$$

where \bar{E}_{K+1} is the diagonal matrix constructed with E_{K+1} and μ is a positive coefficient. The calculated optimal time-varying smoothing boundary layer Θ_{K+1} of the PHUVS system is always a diagonal matrix as $\Theta_{K+1} = \text{diag}((\theta_1)_{K+1} (\theta_2)_{K+1} \cdots (\theta_8)_{K+1})$, and it is a measurement of the disturbance caused by modeling uncertainty and noise as well.

Compare the calculated VBL ψ_{K+1} with a threshold Θ_S which is determined based on prior knowledge of system; when $\Theta_{K+1} \leq \Theta_S$, the optimal VBL-based gain is calculated as

$$K_{K+1} = H_{K+1}^+ \bar{E}_{K+1} \Theta_{K+1}^{-1}. \quad (21)$$

It means that the optimality of estimation can be pursued by this VBL-based gain when the interference is

limited. When $\Theta_{K+1} > \Theta_S$, the interference is considered serious and the conservative SVSF gain is switched to maintain the robustness of estimation as follows:

$$K_{K+1} = H_{K+1}^+ \text{diag} \left[E_{K+1} \circ \text{Sat} \left(\frac{e_{Z,K+1|K}}{\Theta} \right) \right] \times [\text{diag}(e_{Z,K+1|K})]^{-1}, \quad (22)$$

where $\text{Sat}(\cdot)$ represents a saturation function [34, 35] and $\Theta \in \mathbb{R}^{8 \times 1}$ is the standard boundary layer in SVSF. The a posteriori state error covariance matrix can be updated by the selected filtering gain K_{K+1} as

$$P_{K+1|K+1} = (I - K_{K+1}H_{K+1})P_{K+1|K}(I - K_{K+1}H_{K+1})^T + K_{K+1}V_{K+1}K_{K+1}^T. \quad (23)$$

Finally, the estimated state vector $\hat{X}_{K+1|K+1}$ can be obtained by filtering gain:

$$\hat{X}_{K+1|K+1} = \hat{X}_{K+1|K} + K_{K+1}e_{Z,K+1|K}. \quad (24)$$

Although switching between the optimal VBL-based gain and the robust SVSF gain can achieve a balance between optimality and robustness in theory, the decrease in filtering accuracy caused by measurement noise still cannot be ignored. In addition, inappropriate gain switching threshold Θ_S will affect the accuracy as well. Thus, $\hat{X}_{K+1|K+1}$ can be considered as a conservative suboptimal estimation of the state vector of system. The relationship between the desired state vector X_{K+1} and the suboptimal estimated state vector can be defined as

$$X_{K+1|K+1} = \hat{X}_{K+1|K+1} + e_{\hat{X}_{K+1|K+1}}, \quad (25)$$

where $e_{\hat{X}_{K+1|K+1}}$ is the unknown estimation error caused by the measurement noise of system. In order to realize an accurate estimation of the state vector and improve the robustness to unknown disturbances, a generalized RBF NN is integrated into the VBL-SVSF method. This RBF NN has a convincing ability to fit nonlinear mapping relationships and shows excellent training speed and accuracy. It is designed to play the role as a corrector for estimating and compensating the estimation error $e_{\hat{X}_{K+1|K+1}}$.

As illustrated in Figure 2, RBF NN has a three-layer structure including input layer and hidden layer and output layer. Each neuron of the hidden layer is connected to all neurons of the input layer, and the output of the i th hidden layer neuron is calculated by a basis function as

$$n_i = f(\Psi_k, \Phi_i), \quad (26)$$

where $\Psi_k \in \mathbb{R}_{l \times 1}$ is the input vector of the k th training sample and Φ_i is the center of the basis function. The Gaussian basis function is defined as

$$f(\Psi_k, \Phi_i) = \exp \left(-\frac{1}{2\sigma^2} \|\Psi_k - \Phi_i\| \right), \quad (27)$$

where σ represents the standard deviation of the basis function. $\|\Psi_k - \Phi_i\|$ denotes the Euclidean distance between the input vector Ψ_k and the center of basis function Φ_i , and it can be obtained as

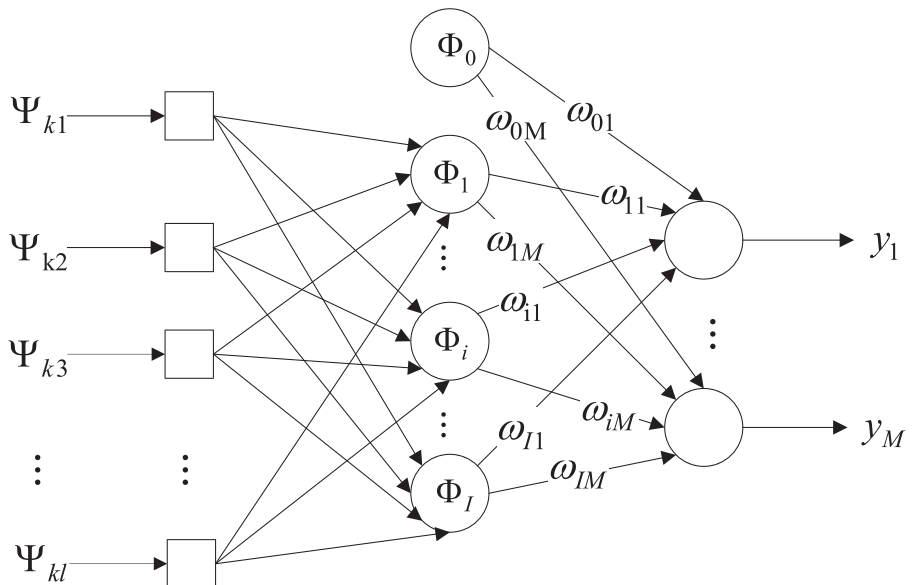


FIGURE 2 The structure of RBF neural network

$$\|\Psi_k - \Phi_i\| = (\Psi_k^T - \Phi_i^T)(\Psi_k - \Phi_i). \quad (28)$$

The output of the output layer neuron is the weighted linear sum of the output of each hidden layer neuron. For example, at the k th training sample, the output of the j th output layer neuron is calculated as

$$y_{kj} = \omega_0 + \sum_{i=1}^I \omega_{ij} n_i. \quad (29)$$

where ω_0 is an additional adjustable threshold. ω_{ij} is the connection weight between the i th hidden layer neuron and the j th output layer neuron. Mature parameter learning algorithms, including regularization method [41], fast hybrid method [42], and gradient descent method, can be adopted to determine the center of basis function Φ and update the connection weights ω between the hidden layer and the output layer. The gradient descent method is realized through the following iterative process:

$$\Gamma = \frac{1}{2} \sum_{n=1}^N \sum_{m=1}^M (d_{nm} - y_{nm})^2, \quad (30)$$

$$\omega_{ij}(k+1) = \omega_{ij}(k) - \eta_1 \frac{\partial \Gamma}{\partial \omega_{ij}(k)}, \quad (31)$$

$$\Phi_i(k+1) = \Phi_i(k) - \eta_2 \frac{\partial \Gamma}{\partial \Phi_i(k)}, \quad (32)$$

where d_{nm} and y_{nm} are the desired output and the actual output of m th output layer neuron with n th training sample, respectively, η_1 and η_2 are the learning rates. The gradient descent method may encounter the problem of local minimum. When its fitting ability is not satisfactory, regularization method and fast hybrid method can be adopted instead.

The complete robust filtering scheme assisted by RBF NN is illustrated in Figure 3. The inputs of this NN-based state error corrector is designed as

$$\Psi_{K+1} = \begin{bmatrix} \overline{\Theta}_{K+1}^T & e_{\hat{X}_{K+1}}^T & e_{Z,K+1|K}^T \end{bmatrix}^T, \quad (33)$$

where $\overline{\Theta}_{K+1}$ is a column vector constructed by the diagonal elements of the optimal time-varying smoothing boundary layer Θ_{K+1} . $e_{\hat{X}_{K+1}}$ is defined as the difference between the estimated state vectors of two adjacent periods:

$$e_{\hat{X}_{K+1}} = \hat{X}_{K+1|K+1} - \hat{X}_{K+1|K} = \hat{X}_{K+1|K+1} - Z^{-1} \hat{X}_{K+1|K+1}, \quad (34)$$

where Z^{-1} represents a unit of time delay. $e_{Z,K+1|K}$ is the residuals vector of system introduced in Equation 16. The output of this state error corrector is $\hat{e}_{\hat{X}_{K+1|K+1}}$ which is considered as an estimation of $e_{\hat{X}_{K+1|K+1}}$ in Equation 25. Thus, the optimal estimated state estimation based on this NN-assisted robust filtering scheme is denoted as

$$\tilde{X}_{K+1|K+1} = \hat{X}_{K+1|K+1} + \hat{e}_{\hat{X}_{K+1|K+1}}, \quad (35)$$

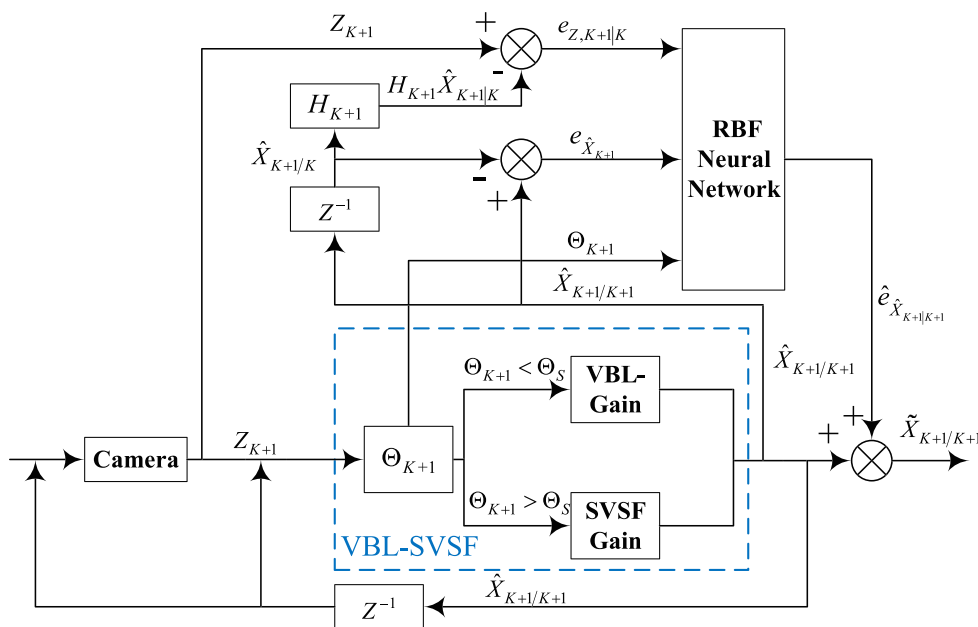


FIGURE 3 The block diagram of neural-network-assisted robust filtering scheme

where the estimation error caused by measurement error of image features has been compensated. According to $\tilde{X}_{K+1|K+1}$, the more accurate estimated total Jacobian can be obtained and the performance of the PHUVS system can be improved as well.

4 | ADAPTIVE SERVO GAIN WITH Q-LEARNING

The convergence speed, positioning accuracy, and stability of the system are affected by the servo gain λ . Thus, a self-adjusting adaptive servo gain is a feasible solution of this problem. The Q-learning strategy that does not require complex rules and detailed prior knowledge of the environment is the most suitable choice for adaptive adjustment of the servo gain [40, 43]. In this section, a novel Q-learning strategy is proposed to adjust the servo gain of the PHUVS system and its details are introduced as follows.

4.1 | Q-table and updating law

Q-learning establishes a mapping relationship, which refers to how much reward value will be obtained when taking a certain action a in a certain state S_e . This mapping relationship can be summarized as a Q-table and the reward value of the state-action pair is defined as $Q(S_e, a)$. During training, the $Q(S_e, a)$ is continuously updated until a converged Q-table is obtained and the update law of the $Q(S_e, a)$ is denoted by

$$Q_{k+1}(S_e^k, a_k) = Q_k(S_e^k, a_k) + \beta \left[r + \gamma \max_{a_{k+1}} Q_k(S_e^{k+1}, a_{k+1}) - Q_k(S_e^k, a_k) \right], \quad (36)$$

where β represents the learning rate and $0 \leq \beta \leq 1$; γ is a reward factor and $0 \leq \gamma \leq 1$. The r is determined through a well-designed reward function. After taking action a_k in state S_e^k , the state reaches S_e^{k+1} and $\max_{a_{k+1}} Q_k(S_e^{k+1}, a_{k+1})$ is the maximum reward value that can be achieved in state S_e^{k+1} by taking an action a_{k+1} .

In actual application, the optimal strategy of adaptive adjustment of servo gain is achieved as

$$\pi(S_e^k) = \arg \max_a Q(S_e^k, a), \quad (37)$$

which means that the action is selected with the maximum reward value in each state according to the converged Q-table.

4.2 | Selection and partition of state space

In our proposed PHUVS system, a controller that directly controls the robot joints based on the estimated total Jacobian matrix is designed. Due to this issue, when the robot has much degrees of freedom, the dimension of the gain matrix will become very large. If different gains are used in each dimension of the gain matrix and independent Q-learning strategy is designed to adjust each gain, it will cause a great workload. Thus, a servo gain matrix λ which is consistent in all dimensions is adopted as

$$\lambda = \begin{bmatrix} \lambda_1 & \cdots & 0 \\ \vdots & \ddots & \vdots \\ 0 & \cdots & \lambda_n \end{bmatrix}_{n \times n}, \lambda_1 = \lambda_2 = \cdots = \lambda_n. \quad (38)$$

And a Q-learning strategy is designed to adjust the gain a in all dimensions simultaneously.

The gain matrix is closely related to the task function error and total Jacobian. Considering the problem of computational complexity and dimension matching, task function error is inappropriate to being selected as the state space of Q-learning. Instead, the inner product of task function error s is chosen as the state space

$$S_e = \{S_e | S_e = s^T s\}. \quad (39)$$

According to the distribution characteristics of the norm of task function error $s^T s$ during servo process, partition method of state space is designed. The interval in the middle of the state space can be divided as follows:

$$S_e^{i+1} = \{S_{\max} \times 10^{-i}, S_{\max} \times 10^{-i+1}\}, i = 1, 2, \dots, n-1, \quad (40)$$

where S_{\max} represents the order of magnitude of the maximum value of $s^T s$ and n is the corresponding orders of the magnitude. The intervals at the beginning and the end of state space are defined as

$$S_e^1 = \{S_{\max}, +\infty\}, \quad (41)$$

$$S_e^{n+1} = \{0, S_{\max} \times 10^{-n+1}\}. \quad (42)$$

4.3 | Action space and reward function

Servo gain is the target to be adjusted by Q-learning, and it is naturally chosen as the action space. An excessive servo gain will lead to the instability of system, and the

resulting violent movement of the robot can even damage the mechanical structure of the system. Conversely, a too small servo gain will make the convergence time of the system too long and reduce the efficiency of the system. Thus, an action set with m gains is given as the action set $a = \{a_i | i = 1, \dots, m\}$.

ϵ -greedy strategy is adopted to determine the corresponding actions during the training of Q-learning. This strategy is an improvement of the greedy strategy, in order to explore more possible actions. It chooses actions according to the maximum value of Q-table with a probability of $1-\epsilon$ and randomly choose actions with a probability of ϵ . The probability ϵ is defined as $\epsilon = \mu^n$, where μ is a constant probability and n is the number of training times. This means that at the beginning of training, more random actions are selected to explore more possibilities. As the training progresses, the value of the Q-table becomes more and more convincing, so more select actions based on the Q-table.

The purpose of adjusting the servo gain is to accelerate the convergence speed without affecting the performance of system. Thus, the reward function is designed separately based on the following two different conditions

1. When the task function is moving away from the desired value after selecting an inappropriate servo gain, a worst reward value should be given as a penalty to avoid choosing this gain again.
2. When the task function is approaching the desired value, a changing reward value should be given. The closer the current task function is to the desired value, the better the value of the reward function should be determined.

In summary, the reward function is designed as

$$r = \begin{cases} -5r_0, & \text{if } \Delta s > 0 \\ -r_0 [(s_k^T s_k) / (s_0^T s_0)]^{1/2}, & \text{else,} \end{cases} \quad (43)$$

where r_0 is a constant positive value and s_0 is the initial value of the task function error. s_k is the norm of task function error in the k th iteration of the training process and Δs is defined as $\Delta s = s_k^T s_k - s_{k-1}^T s_{k-1}$.

5 | THE FRAME OF PHUVS WITH NN-ASSISTED FILTERING SCHEME AND Q-LEARNING

The frame of this PHUVS system is illustrated in Figure 4. A discrete proportional controller is designed as

$$\Delta q = -\lambda J_t^+ s, \quad (44)$$

where Δq is the joint angle increment obtained by discretizing the joint velocities \dot{q} through sampling time ΔT . J_t^+ is the Moore–Penrose pseudoinverse of the total Jacobian J_t estimated by this proposed NN-assisted filtering scheme. The singularity and ill-condition problems of the total Jacobian that may appear in the servo process can be dealt with by the singular value filtering method [23]. λ is the adaptive servo gain adjusted by the proposed Q-learning strategy.

The training sample set of this RBF-NN-based corrector is obtained through the original VBL-SVSF cycle and the RBF NN is trained offline. The norm of task function error $s^T s$ in the PHUVS system is adopted as the real-time state in the training of Q-learning and the reward function is calculated by the task function error s as well. Trained with the proposed PHUVS system, a converged Q-table can be obtained for adaptive adjustment of servo gain.

In addition, the estimated initial total Jacobian J_t can be calculated by performing several trial movements as $J_0 = [\Delta h^1, \Delta h^2, \dots, \Delta h^n]_{8 \times n} [\Delta q^1, \Delta q^2, \dots, \Delta q^n]_{n \times n}^{-1}$. $\Delta h^1, \Delta h^2, \dots, \Delta h^n$ are the corresponding change in task function brought by n steps linearly independent trial movement $\Delta q^1, \Delta q^2, \dots, \Delta q^n$.

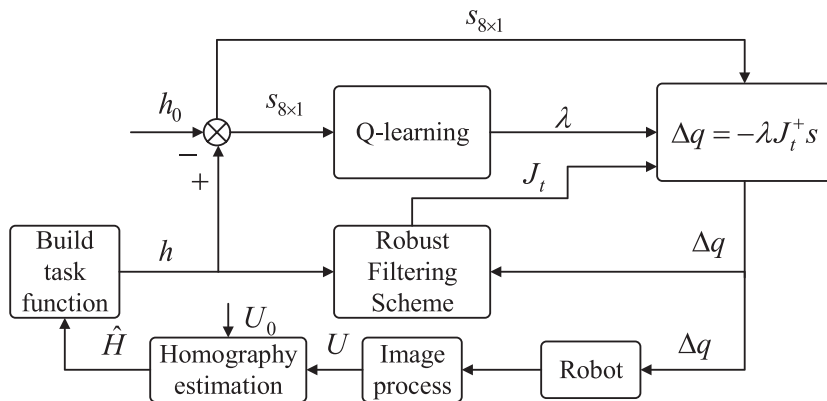


FIGURE 4 The structure of our proposed PHUVS system

6 | RESULTS AND DISCUSSIONS

6.1 | Simulations

In this section, several simulations are carried out to verify our proposed PHUVS method with NN-assisted robust filtering scheme and Q-learning. The simulation system consists of a 9-DOF manipulator independently designed by our team and an eye-in-hand camera with a resolution of 1280×960 . The structure of the manipulator is shown in Figure 5, and the DH parameters of the manipulator are given in Table 1. Various settings of the simulations, such as target size and measurement errors of image features, are set according to the actual working conditions

TABLE 1 D-H parameters of 9-DOF manipulator

Joint	q_n	α_{n-1}	a_{n-1}	d_n	Limit
1	q_1	0	0	0	$\pm 90^\circ$
2	q_2	90°	165.5	0	$\pm 90^\circ$
3	q_3	-90°	165.5	0	$\pm 90^\circ$
4	q_4	90°	165.5	0	$\pm 90^\circ$
5	q_5	-90°	165.5	0	$\pm 90^\circ$
6	q_6	90°	165.5	0	$\pm 90^\circ$
7	q_7	-90°	165.5	0	$\pm 90^\circ$
8	q_8	90°	165.5	0	$\pm 90^\circ$
9	q_9	-90°	165.5	0	$\pm 90^\circ$

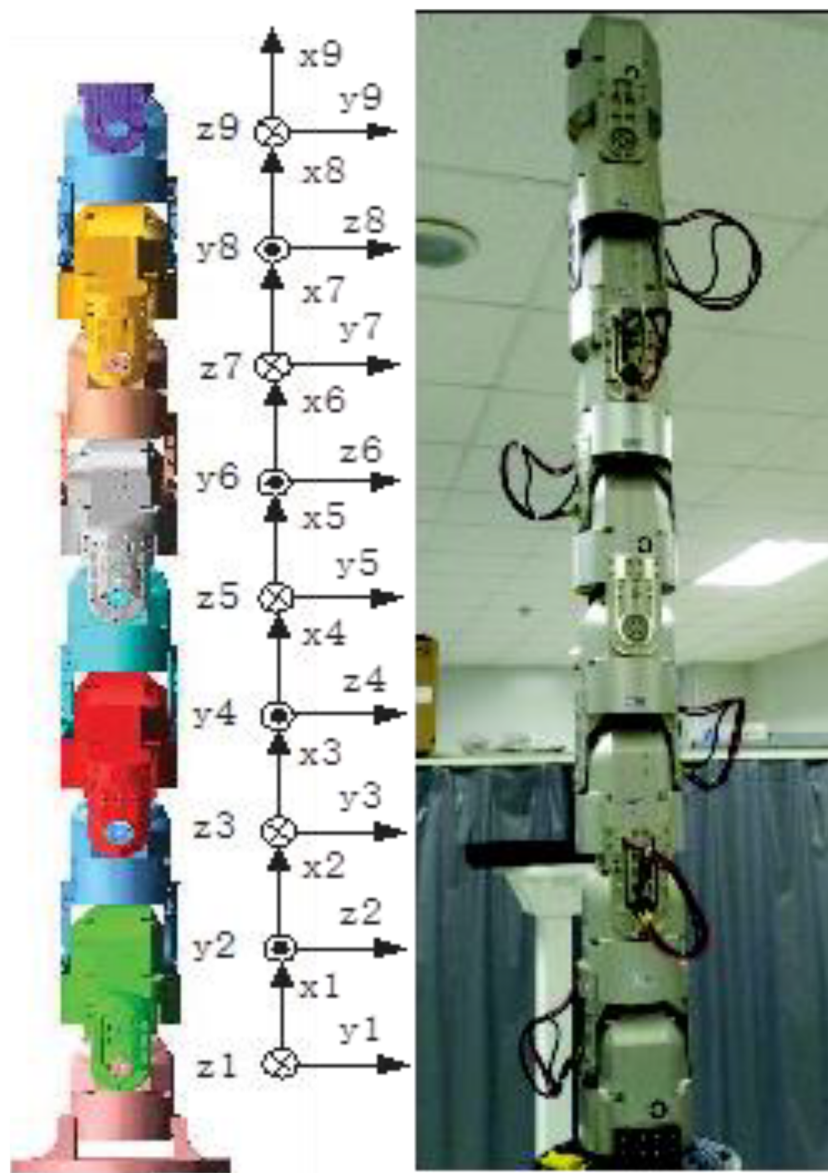


FIGURE 5 Manipulator structure and link coordinate systems of 9-DOF manipulator

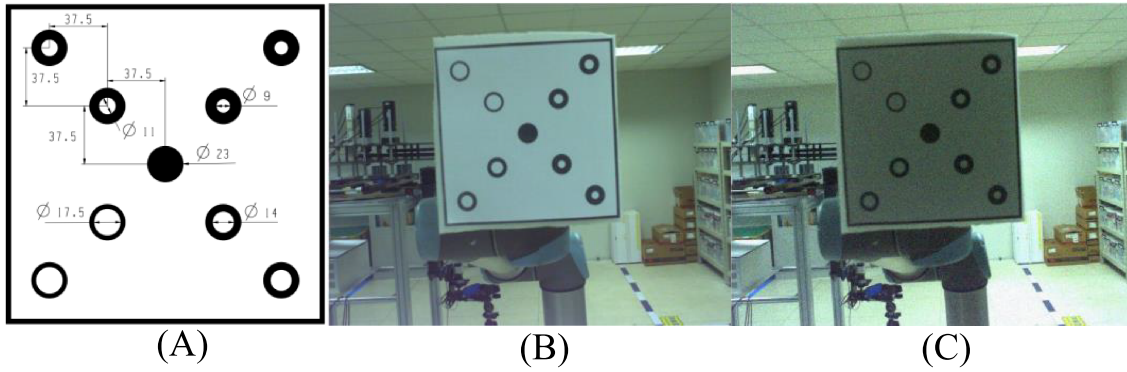


FIGURE 6 (A) Design drawing of the target, (B) target image collected in a normal environment, (C) target image collected in a noisy environment with insufficient light

in order to simulate the performance of the system under actual working conditions [44]. As shown in Figure 6A, the target is composed of multiple rings, and the center of the ring is used as the feature points. According to affine invariance, the ratio of the inner ring to the outer ring and the distance from the solid circle in the middle are used to encode the feature points. As shown in Figure 6B, clear image of the target can be obtained in a well-lit laboratory environment with low noise, and the sufficiently accurate measurement of feature points can be obtained based on multiple measurements and averaging by using robust ideal feature fitting method [44]. However, as shown in Figure 6C, when the interference caused by illumination and image noise existed, the measurement error of image features cannot be ignored. In order to test the performance of the proposed method, random measurement errors of image feature with different statistical characteristics are added during the simulations.

The training sample set of the RBF NN is collected from simulations of the VBL-SVSF method. The optimal time-varying smoothing boundary layer $\Theta_{K+1} \in \mathbb{R}^{8 \times 1}$, state estimation increment $e_{\hat{X}_{K+1}} \in \mathbb{R}^{72 \times 1}$, system residuals vector $e_{Z,K+1|K} \in \mathbb{R}^{8 \times 1}$, and the corresponding output $e_{\hat{X}_{K+1|K+1}} \in \mathbb{R}^{72 \times 1}$ can be obtained in each iteration of these simulations. In this paper, a total of 557 pairs of input-output samples are collected to train the NN. According to the dimension of the task function and the DOF of the manipulator, the input layer of the NN is a fixed structure with 88 neurons and the output layer has 72 neurons. After the training of NN, a hidden layer with 500 neurons is obtained and the mean square error between the desired output and the actual output can reach 1.2×10^{-6} which demonstrates the convincing fitting ability of the trained RBF NN to training samples set.

The main purpose of visual servo is to control the end effector of manipulator move from the initial pose to the

desired pose. Performances under different initial pose errors including pure translation, pure rotation, and general motion will be simulated.

1. Pure translation: The initial pose error between the initial pose and the desired pose of the manipulator is defined as

$$[\Delta x \ \Delta \theta] = [-230mm \ 150mm \ 350mm \ 0^\circ \ 0^\circ \ 0^\circ].$$

2. Pure rotation: The initial pose error between the initial pose and the desired pose of the manipulator is defined as

$$[\Delta x \ \Delta \theta] = [0 \ 0 \ 0 \ -10^\circ \ -20^\circ \ 45^\circ].$$

3. General motion: The initial pose error between the initial pose and the desired pose of the manipulator is defined as

$$[\Delta x \ \Delta \theta] = [-450mm \ 260mm \ 100mm \ -30^\circ \ -5^\circ \ 36^\circ].$$

The positioning error after the task function converges is the most typical indexes to compare different visual servo systems [21]. Therefore, translation error x_e and orientation error θ_e are selected as the performance index to verify the superiority of our proposed method. In order to test the robustness in the actual working environment, different levels of positioning errors of image features are added in each simulation according to actual condition. The gain switching threshold of

the VBL-SVSF method is defined as $\Theta_{K+1} = 10^3 \times \text{diag}(1 \ 1 \ 5 \ 1 \ 1 \ 5 \ 0.1 \ 0.1)$ and an optimal fixed servo gain $\lambda = 0.02$ is selected after several attempts. In order to make the test results more reasonable and convincing, take the mean values of 50 simulations as the test result for comparison.

The positioning error of the KF method, VBL-SVSF method, and proposed method in different initial pose error are tested under different statistical characteristics of measurement error of image features. All the test results of the three methods are shown in Table 2. $|V|$ represents the mean value of the measurement errors of image and σ represents the standard deviation. It's obvious that our proposed method shows the most convincing performance. The proposed method shows the best positioning accuracy than the KF method and VBL-SVSF method regardless of the statistical characteristics of measurement errors of image feature. This is because the statistical characteristics of the system measurement noise caused by the measurement error of the image feature points are difficult to determine. Thus, the optimality of the KF method will be lost and its accuracy for estimating the total Jacobian matrix will be greatly reduced as well. The VBL-SVSF method shows better accuracy than the KF method by introducing the optimal time-varying smoothing boundary layer into the SVSF method. However, its performance in positioning accuracy is still insufficient. Compared with VBL-SVSF method, our proposed robust filtering scheme introduces an RBF NN to play the role of a corrector to compensate the estimation error caused by measurement noise. According to the test results, its better performance in accuracy and robustness can be verified.

The interference of measurement noise on the servo process cannot be ignored as well, especially in the case of large initial pose error that combine translation error and rotation error. Taking the above case of general motion as an example, the performance of each method under different levels of features measurement errors was simulated. As shown in Figure 7, when measurement errors of image features with $|V| = 0.08$ and $\sigma = 0.1$ are added, the camera trajectories in Cartesian space and the feature trajectories in the image plane of all the three methods are still smooth. In Figure 8A,B, when the simulations are carried out under measurement errors of image features with $|V| = 0.12$ and $\sigma = 0.15$, although all three methods can successfully converge, the feature trajectories and the camera trajectories of both the KF method and VBL-SVSF method show obvious disturbances. In comparison, as shown in Figure 7C, our proposed robust filtering scheme maintains smooth image trajectory and camera trajectory, which proves the anti-interference ability of our proposed method. When the measurement errors of image features are increased to $|V| = 0.16$ and $\sigma = 0.2$, the fluctuations of the feature trajectory and camera trajectory of the KF method and the VBL-SVSF method have become more serious as shown in Figure 9. In actual work, such fluctuations will bring many undesirable effects to the system which may result in the failure of the servo task, and sometimes it may even result in the damage to the mechanical structure of the visual servo system. Therefore, these fluctuations should be avoided as much as possible. As can be seen in Figure 8C, our proposed method not only has a better feature trajectory in image plane but also a smooth camera trajectory in Cartesian space. In other words, our

TABLE 2 Positioning errors of different method

Task	Method	Noise					
		$ V = 0.08, \sigma = 0.1$		$ V = 0.12, \sigma = 0.15$		$ V = 0.16, \sigma = 0.2$	
		x_e	θ_e	x_e	θ_e	x_e	θ_e
Pure translation	KF	0.3651	0.0005	0.7993	0.0021	1.2124	0.0034
	VBL-SVSF	0.1733	0.0002	0.3323	0.0001	0.5338	0.0014
	Proposed method	0.0841	6×10^{-6}	0.1338	4×10^{-5}	0.2279	0.0003
Pure rotation	KF	0.2902	0.0005	0.7403	0.0016	1.3801	0.0029
	VBL-SVSF	0.1834	0.0003	0.3667	0.0009	0.7058	0.0016
	Proposed Method	0.1295	0.0001	0.2532	0.0005	0.5634	0.0012
General motion	KF	0.8946	0.0019	1.3334	0.0030	2.1645	0.0052
	VBL-SVSF	0.5359	0.0012	1.0350	0.0024	1.4724	0.0034
	Proposed method	0.4070	0.0009	0.6979	0.0015	0.8944	0.0020

Note: x_e is in millimeter and θ_e is in radian. Bold values highlight the results of our proposed method.

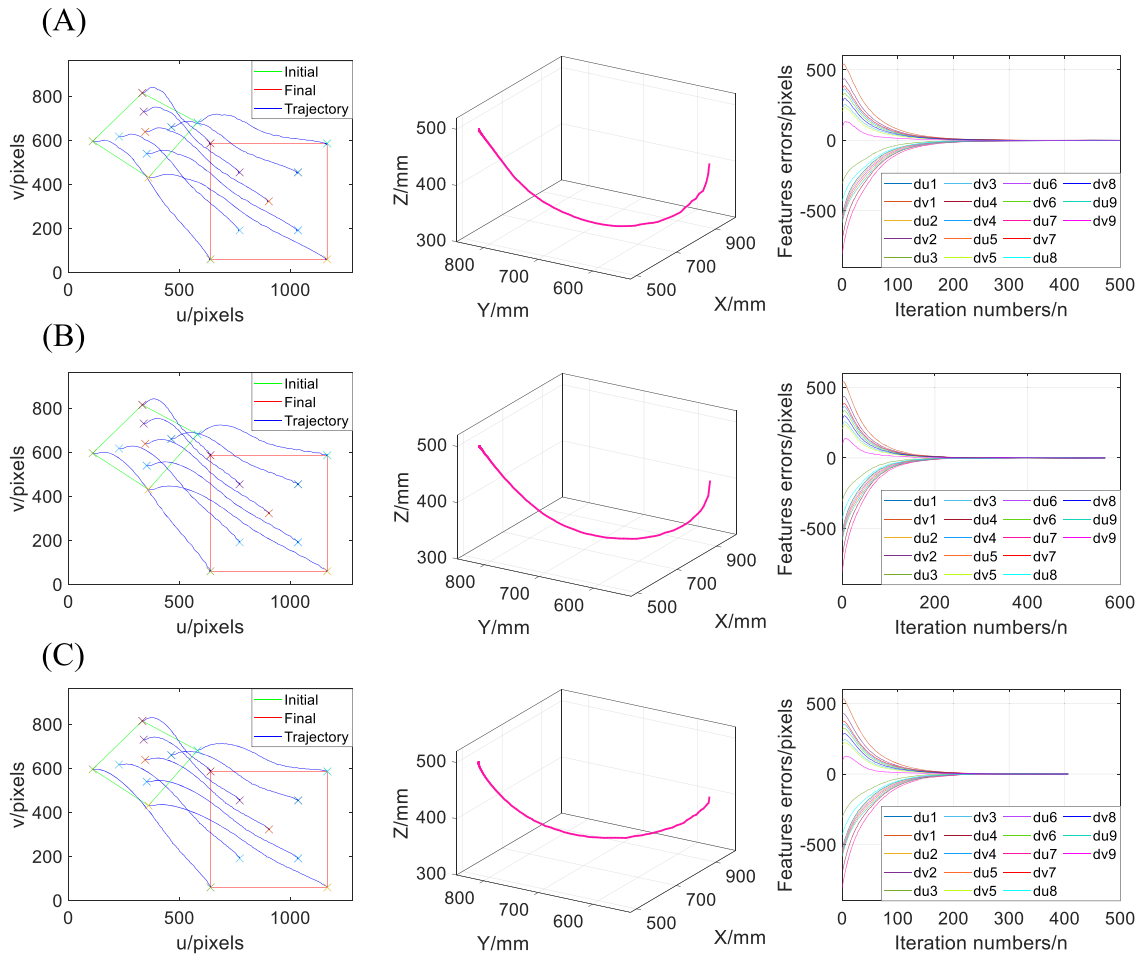


FIGURE 7 Simulation results of general motion case with noise $|V| = 0.08$ and $\sigma = 0.1$. The first, second, and third rows are the results of (A) the KF method, (B) the VBL-SVSF method, and (C) our proposed method, respectively. The first, second, and third columns are (1) image feature trajectories, (2) camera trajectories in Cartesian space, and (3) image feature errors, respectively

proposed filtering scheme suppresses the occurrence of fluctuations in the servo process and shows more convincing anti-interference ability.

In the case of large initial pose error, the selection of servo gain is important. When the task function is far from the desired value, a large servo gain will cause the system to be unstable, while a small servo gain can ensure the stability; when the task function is close to the desired value, a small servo gain will cause the system to converge slowly, while a large servo gain can speed up the convergence and improve the positioning accuracy. Still taking the above case of general motion as an example, the Q-learning strategy is used to adaptively adjust the servo gain of our proposed visual servo system. The state space of Q-learning is divided into six intervals. According to several simulations, the reasonable range of servo gain is roughly determined, and the action set is designed in a uniformly distributed manner as

$$a = \{0.02 \ 0.05 \ 0.1 \ 0.15 \ 0.2 \ 0.25 \ 0.3\}.$$

The reward factor is set as $\gamma = 0.8$ to fully consider the current rewards, and the learning rate of Q-learning is selected as $\beta = 0.5$ to balance the existing knowledge and the current rewards. To explore more possibilities, the probability of randomly choosing an action in Q-table is set as $\varepsilon = 0.9^n$, and it will decrease as the number of training n increases. The parameter of reward function is defined as $r_0 = 100$. The training will be iteratively carried out until a convergent Q-table can be obtained. In each episode, if the norm of the task function error is less than a threshold 0.02, the episode will stop and the iteration numbers of servo process will be recorded. The training results of the Q-learning strategy for adaptive servo gain are shown in Figure 10. It represents the change in the number of iterations required for the system to converge during the process of training. The

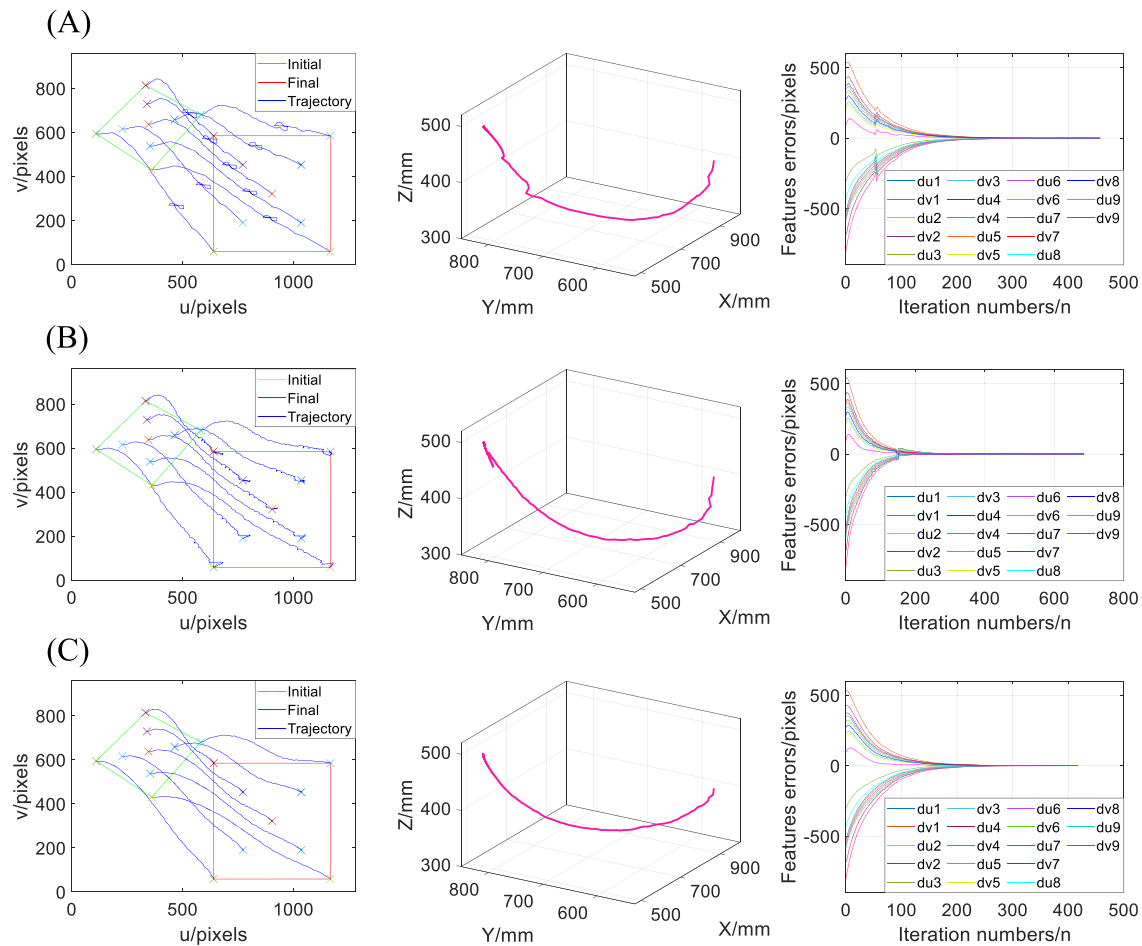


FIGURE 8 Simulation results of general motion case with noise $|V| = 0.12$ and $\sigma = 0.15$. The first, second, and third rows are the results of (A) the KF method, (B) the VBL-SVSF method, and (C) our proposed method, respectively. The first, second, and third columns are (1) image feature trajectories, (2) camera trajectories in Cartesian space, and (3) image feature errors, respectively

Q-table was trained 100 times and converged at the 76th times.

After the training of Q-learning, a convergent Q-table can be obtained for self-adjusting the servo gain during servo process. As in the previous simulation, our proposed system with adaptive servo gain is tested under different level of measurement error of image features. The number of iterations required for the system to converge are listed in Table 3, and the positioning error are shown in Table 4. These results are the mean values of 50 simulations. It's obvious that the system with adaptive servo gain shows faster convergence speed and further improves the positioning accuracy. The performance of the system with adaptive servo gain under different levels of measurement error of image feature is shown in Figure 11. Compared with the system using a fixed gain as shown in Figures 7–9, the system with adaptive gain shows smooth feature trajectory and camera trajectory as

well. However, it achieves convergence with fewer iterations, which is much faster than the system with fixed servo gain. This illustrates that while the adaptive servo gain speeds up the convergence speed, it does not result in the loss of robustness and anti-interference ability. As a conclusion, the advantages of our proposed system with robust filtering scheme and adaptive servo gain can be fully verified.

6.2 | Experiments

In order to evaluate the performance of the proposed method in the actual working environment, experiments based on 9-DOF robot are conducted. As shown in Figure 12, the experimental platform is arranged to simulate the case that achieving the alignment of the two manipulators based on visual servo system. The

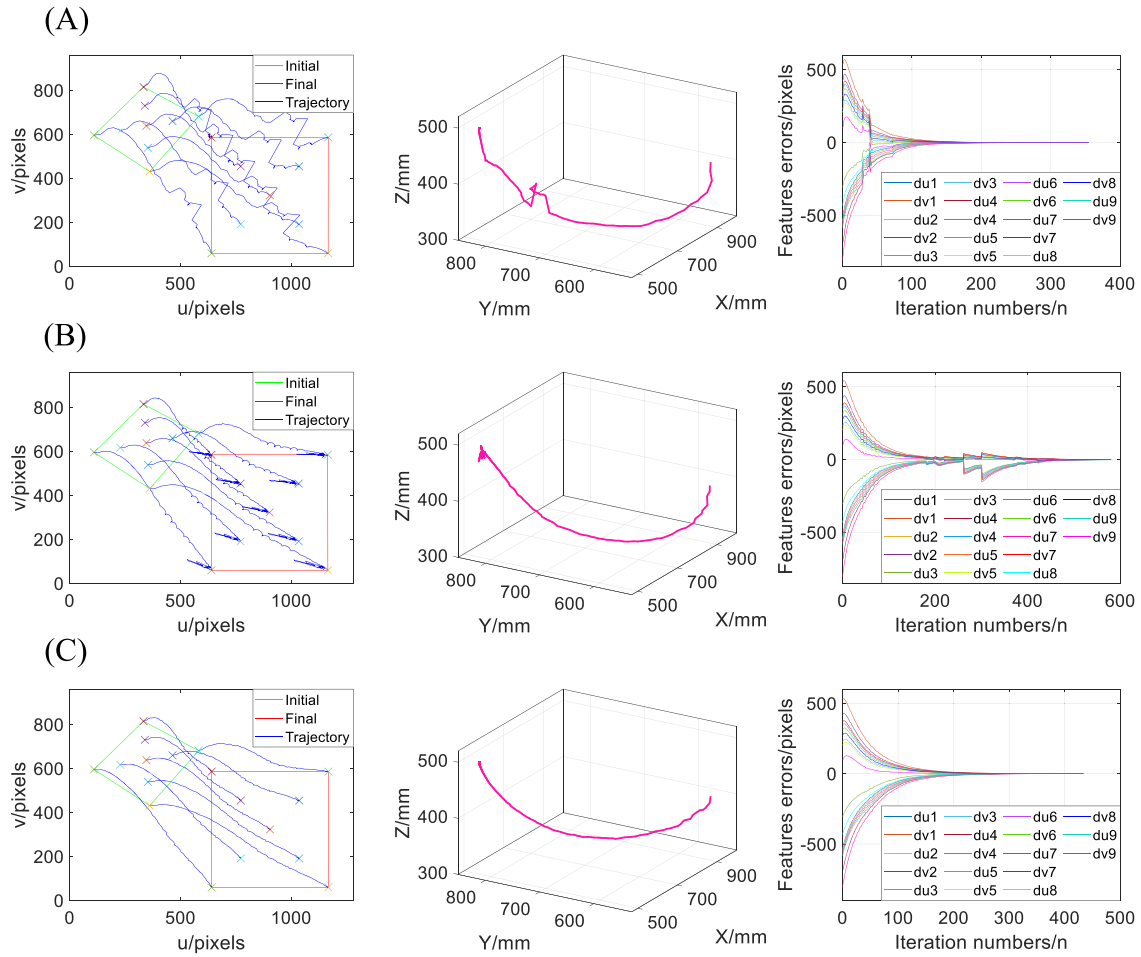


FIGURE 9 Simulation results of general motion case with noise $|V| = 0.16$ and $\sigma = 0.2$. The first, second, and third rows are the results of (A) the KF method, (B) the VBL-SVSF method, and (C) our proposed method, respectively. The first, second, and third columns are (1) image feature trajectories, (2) camera trajectories in Cartesian space, and (3) image feature errors, respectively

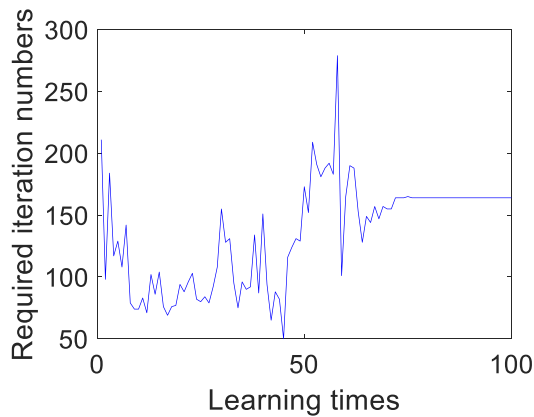


FIGURE 10 Q-learning convergence result for simulation

cooperative target with nine feature points is installed at the end-effector of Universal Robot, and the camera with resolution 1280×960 is mounted at the end-effector of 9-DOF manipulator. In order to simulate the actual working condition, the initial pose error is set to the more common case of general motion that combines translation error and rotation error

$$[\Delta x \ \Delta \theta] = [-250\text{mm} \ 300\text{mm} \ 100\text{mm} \ -30^\circ \ -3^\circ \ 30^\circ].$$

A training sample set that contains 403 pairs of input-output samples is used for training the NN-based corrector. The trained NN has an input layer with 88 neurons, a hidden layer with 350 neurons, and an output layer with 72 neurons. The state space of Q-learning is

TABLE 3 The number of iterations required for the system to converge

Method	Noise		
	$ V = 0.08, \sigma = 0.1$	$ V = 0.12, \sigma = 0.15$	$ V = 0.16, \sigma = 0.2$
Fixed gain	367	402	428
Adaptive gain	176	188	217

Note: Bold values highlight the results of our proposed method.

TABLE 4 Positioning errors

Method	Noise					
	$ V = 0.08, \sigma = 0.1$		$ V = 0.12, \sigma = 0.15$		$ V = 0.16, \sigma = 0.2$	
	x_e	θ_e	x_e	θ_e	x_e	θ_e
Fixed gain	0.4070	0.0009	0.6979	0.0015	0.8944	0.0020
Adaptive gain	0.2436	0.0004	0.3762	0.0007	0.5576	0.0011

Note: x_e is in millimeter and θ_e is in radian. Bold values highlight the results of our proposed method.

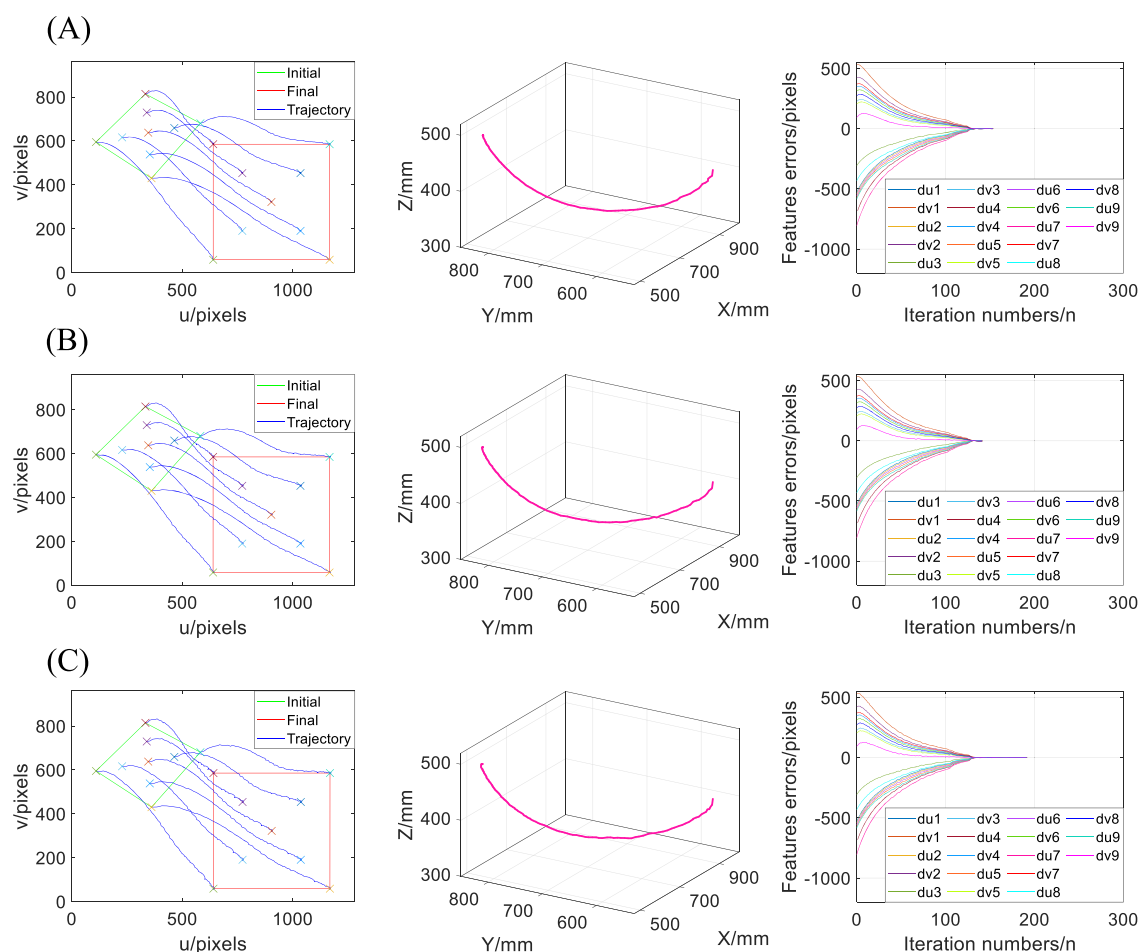


FIGURE 11 Simulation results of our proposed system with adaptive servo gain. 1st, 2nd and 3rd rows are the results with (A) noise $|V| = 0.08$ and $\sigma = 0.1$, (B) noise $|V| = 0.12$ and $\sigma = 0.15$, (C) $|V| = 0.16$ and $\sigma = 0.2$, respectively. The first, second, and third columns are (1) image feature trajectories, (2) camera trajectories in Cartesian space, and (3) image feature errors, respectively



FIGURE 12 Experiment platform

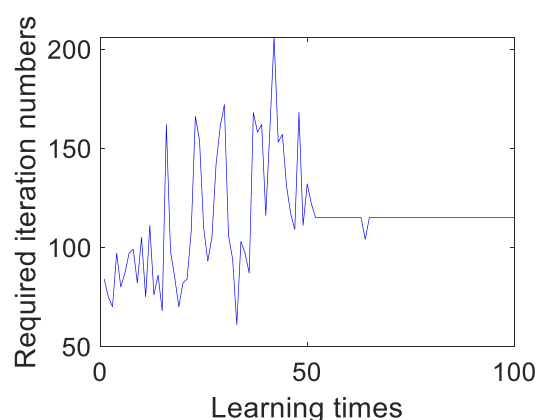


FIGURE 13 Q-learning convergence result for experiment

divided into six intervals. According to the initial error set in the experiments, the action set of Q-learning is designed as

$$a = \{0.02 \ 0.05 \ 0.1 \ 0.15 \ 0.2 \ 0.25 \ 0.3\}.$$

The training of Q-learning is carried out in simulation environment, and then the obtained convergent Q-table is applied to the experiment. The parameters of Q-learning are the same as in simulation, and the training

process are shown in Figure 13. The Q-table was trained 100 times and converged at the 65th time.

The experiments were carried out in two cases. In case 1, these methods are tested in a normal laboratory environment. In case 2, interference was added by adjusting the light condition in environment. All test results in two cases are shown in Table 5, and the results are the mean value of 10 tests. In actual experiments, due to the various slight errors in the system, the positioning error appears to be more serious than simulations. However, our proposed method still shows better positioning accuracy than the KF method and VBL-SVSF method. The performances of these methods under two different cases are shown in Figures 14 and 15. In case 1, the camera trajectories in Cartesian space and the feature trajectories in the image plane of all these methods are still acceptable. However, in case 2, the camera trajectories and the feature trajectories of the KF method and VBL-SVSF method are obviously affected. The performance of our proposed method is still acceptable and show relatively smooth feature trajectory and camera trajectory. Thus, the robustness of the proposed method can be verified. The performance of our proposed system with adaptive servo gain adjusted by Q-learning can be seen in Table 5 and Figures 14 and 15. The average number of iterations required for the system to converge is shown in Table 6. Obviously, compared with the system with fixed servo

TABLE 5 Positioning errors

Method	Normal environment		Noisy environment	
	x_e	θ_e	x_e	θ_e
KF	3.252	0.014	5.163	0.021
VBL-SVSF	2.761	0.013	4.048	0.018
Proposed method with fixed gain	2.226	0.011	3.021	0.014
Proposed method with adaptive gain	2.184	0.011	2.973	0.014

Note: x_e is in millimeter and θ_e is in radian. Bold values highlight the results of our proposed method.

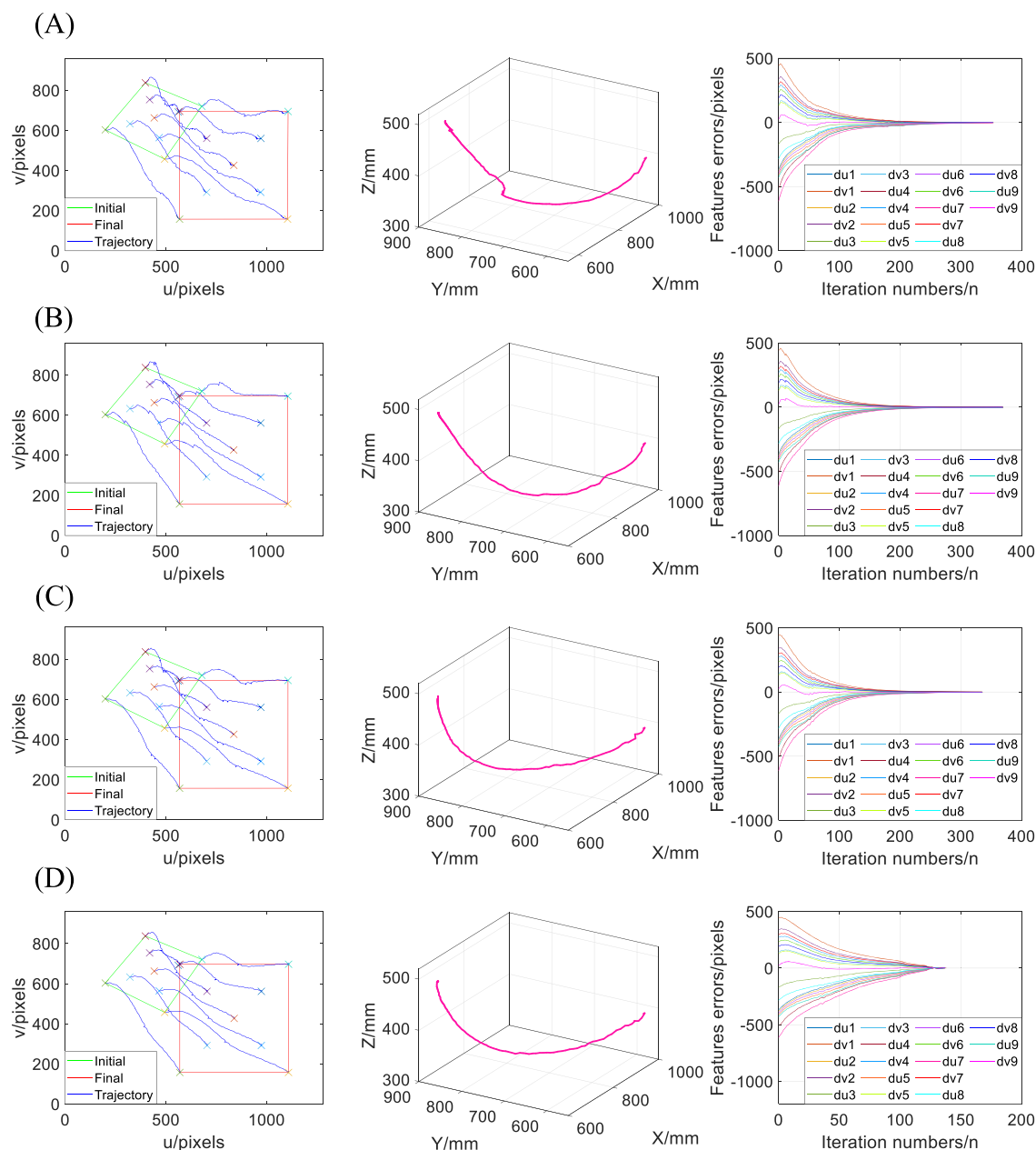


FIGURE 14 Experiment results in normal environment. The first, second, third, and fourth rows are the results of (A) the KF method, (B) the VBL-SVSF method, (C) our proposed method, and (D) our proposed method with adaptive servo gain, respectively. The first, second, and third columns are (1) image feature trajectories, (2) camera trajectories in Cartesian space, and (3) image feature errors, respectively

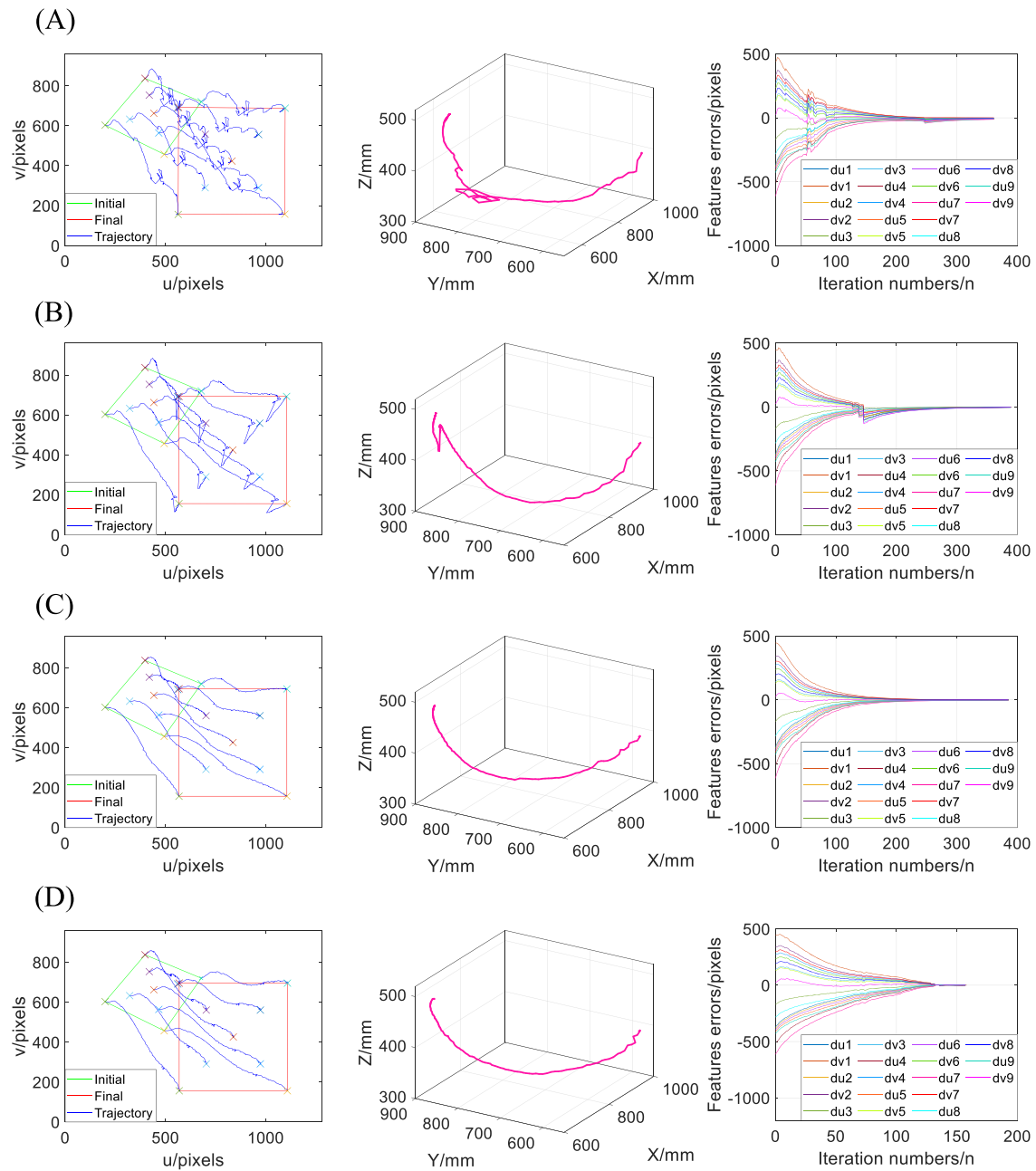


FIGURE 15 Experiment results in noisy environment. The first, second, third, and fourth rows are the results of (A) the KF method, (B) the VBL-SVSF method, (C) our proposed method, and (D) our proposed method with adaptive servo gain, respectively. The first, second, and third columns are (1) image feature trajectories, (2) camera trajectories in Cartesian space, and (3) image feature errors, respectively

TABLE 6 The number of iterations required for the system to converge

Method	Normal environment	Noisy environment
Fixed gain	327	402
Adaptive gain	129	154

Note: Bold values highlight the results of our proposed method.

gain, the system with adaptive servo gain shows a faster convergence speed while maintaining the robustness.

7 | CONCLUSIONS

In this paper, a homography-based uncalibrated visual servo system with NN-assisted robust filtering scheme

and adaptive servo gain is introduced. This system adopts a homography-based task function with robustness to image defects, and a discrete controller based on estimated total Jacobian that directly controls robot joints is designed for obtaining the robustness to robot parameter errors. The proposed NN-assisted robust filtering scheme can estimate the total Jacobian between task function and robot joints without system calibration, which means robustness to calibration errors. In addition, compared with original filtering methods, this scheme combined with NN-based corrector shows better accuracy and convincing anti-interference ability against the measurement errors of image features. Then, a novel Q-learning strategy for the proposed PHUVS system is proposed to make adaptive adjustment for the servo gain. This adaptive gain enables the system to obtain a faster convergence rate while maintaining stability. At last, several simulations and experiments are carried out and the results verify the better performance of the proposed filtering scheme and adaptive servo gain.

ACKNOWLEDGMENTS

This research was funded by the National Natural Science Foundation of China under Grant 11672290 and 11972343; Jilin Scientific and Technological Development Program under Grant 2018020102GX; and Jilin Province and Chinese Academy of Sciences Cooperation in Science and Technology High-Tech Industrialization Special Funds Project under Grant 2018SYHZ0004.

AUTHOR CONTRIBUTIONS

Jinlin Gu: Conceptualization; formal analysis, methodology, software, validation. **Wenrui Wang:** Formal analysis. **Ang Li:** Software, visualization. **Mingchao Zhu:** Funding acquisition, project administration, resources. **Lihua Cao:** Resources. **Zhenbang Xu:** Project administration; resources.

ORCID

Mingchao Zhu  <https://orcid.org/0000-0003-3579-7956>

REFERENCES

1. J. T. Guillén-Bonilla, C. C. Vaca García, S. Di Gennaro, M. E. Sánchez Morales, and C. Acosta Lúa, *Vision-based nonlinear control of quadrotors using the photogrammetric technique*, *Math. Probl. Eng.* **2020** (2020), 1–10. <https://doi.org/10.1155/2020/5146291>
2. H. Xie, A. F. Lynch, K. H. Low, and S. Mao, *Adaptive output-feedback image-based visual servoing for quadrotor unmanned aerial vehicles*, *IEEE Trans. Control Syst. Technol.* **28** (2020), 1034–1041.
3. G. Allibert, M. D. Hua, S. Krupinski, and T. Hamel, *Pipeline following by visual servoing for autonomous underwater vehicles*, *Control Eng. Pract.* **82** (2019), 151–160.
4. F. Bonin-Font and A. Burguera Burguera, *NetHALOC: A learned global image descriptor for loop closing in underwater visual SLAM*, *Expert Syst.* **38** (2020), 1–23. <https://doi.org/10.1111/essy.12635>
5. X. Zhao, Z. Xie, H. Yang, and J. Liu, *Minimum base disturbance control of free-floating space robot during visual servoing pre-capturing process*, *Robotica* **38** (2020), no. 4, 652–668. <https://doi.org/10.1017/S0263574719000924>
6. A. Rivolta, P. Lunghi, and M. Lavagna, *GNC & robotics for on orbit servicing with simulated vision in the loop*, *Acta Astronaut.* **162** (2019), 327–335. <https://doi.org/10.1016/j.actaastro.2019.06.005>
7. G. Dong and Z. H. Zhu, *Position-based visual servo control of autonomous robotic manipulators*, *Acta Astronaut.* **115** (2015), 291–302. <https://doi.org/10.1016/j.actaastro.2015.05.036>
8. F. T. Colombo, J. V. de Carvalho Fontes, and M. M. da Silva, *A visual servoing strategy under limited frame rates for planar parallel kinematic machines*, *J. Intell. Robot. Syst.: Theory Appl.* **96** (2019), 95–107. <https://doi.org/10.1007/s10846-019-00982-7>
9. R. Reyes and R. Murrieta-Cid, *An approach integrating planning and image-based visual servo control for road following and moving obstacles avoidance*, *Int. J. Control* **93** (2020), 2442–2456. <https://doi.org/10.1080/00207179.2018.1562225>
10. Z. Zhou, R. Zhang, and Z. Zhu, *Uncalibrated dynamic visual servoing via multivariate adaptive regression splines and improved incremental extreme learning machine*, *ISA Trans.* **92** (2019), 298–314. <https://doi.org/10.1016/j.isatra.2019.02.029>
11. Z. Ma and J. Su, *Robust uncalibrated visual servoing control based on disturbance observer*, *ISA Trans.* **59** (2015), 193–204. <https://doi.org/10.1016/j.isatra.2015.07.003>
12. F. Wang, Z. Liu, C. L. P. Chen, and Y. Zhang, *Robust adaptive visual tracking control for uncertain robotic systems with unknown dead-zone inputs*, *J. Franklin Inst.* **356** (2019), 6255–6279. <https://doi.org/10.1016/j.jfranklin.2019.05.040>
13. E. Malis, F. Chaumette, and S. Boudet, *2-1/2-D visual servoing*, *IEEE Trans. Robot. Autom.* **15** (1999), 238–250. <https://doi.org/10.1109/70.760345>
14. F. Janabi-Sharifi, L. Deng, and W. J. Wilson, *Comparison of basic visual servoing methods*, *IEEE/ASME Trans. Mechatron.* **16** (2011), 967–983.
15. F. Chaumette and S. Hutchinson, *Visual servo control. I. Basic approaches*, *IEEE Robot. Autom. Mag.* **13** (2006), 82–90. <https://doi.org/10.1109/MRA.2006.250573>
16. M. Hao and Z. Sun, *A universal state-space approach to uncalibrated model-free visual servoing*, *IEEE Trans. Mechatron.* **17** (2012), 833–846.
17. J. Zhang and D. Liu, *Calibration-free and model-independent method for high-DOF image-based visual servoing*, *J. Control Theory Appl.* **11** (2013), 132–140.
18. J. Munnae: *Uncalibrated robotic visual servo tracking for large residual problems*, [PhD Thesis]. Georgia Institute of Technology, 2010.
19. J. Gu, W. Wang, M. Zhu, Y. Lv, Q. Huo, and Z. Xu, *Research on a technology of automatic assembly based on uncalibrated visual servo system*, In *Proceedings of 2018 IEEE International Conference on Mechatronics and Automation, ICMA 2018*, IEEE, 2018, 872–877.
20. J. Musić, M. Bonković, and M. Ceci, *Comparison of uncalibrated model-free visual servoing methods for small-*

- amplitude movements: A simulation study*, Int. J. Adv. Robot. Syst. **11** (2014), 108. <https://doi.org/10.5772/58822>
21. Z. Gong, B. Tao, H. Yang, Z. Yin, and H. Ding, *An uncalibrated visual servo method based on projective homography*, IEEE Trans. Autom. Sci. Eng. **15** (2018), 806–817. <https://doi.org/10.1109/TASE.2017.2702195>
 22. Z. Gong, B. Tao, C. Qiu, Z. Yin, and H. Ding, *Trajectory planning with shortest path for modified uncalibrated visual servoing based on projective homography*, IEEE Trans. Autom. Sci. Eng. **17** (2020), 1076–1083. <https://doi.org/10.1109/tase.2019.2954598>
 23. J. Gu, M. Zhu, L. Cao, A. Li, and W. Wang, *Improved uncalibrated visual servo strategy for hyper-redundant manipulators in on-orbit automatic assembly*, Appl. Sci. **10** (2020), 6968. <https://doi.org/10.3390/app10196968>
 24. J. A. Piepmeyer and H. Lipkin, *Uncalibrated eye-in-hand visual servoing*, Int. J. Robot. Res. **22** (2003), no. 10–11, 805–819.
 25. K. Hosoda and M. Asada, *Versatile visual servoing without knowledge of true Jacobian*, In *Proceedings of the IEEE/RSJ/GI Conference Intelligent Robots and Systems*, IEEE, 1994, 186–193.
 26. F. Wang, F. Sun, J. Zhang, B. Lin, and X. Li, *Unscented particle filter for online total image Jacobian matrix estimation in robot visual servoing*, IEEE Access **7** (2019), 92020–92029.
 27. X. Zhong, X. Zhong, and X. Peng, *Robots visual servo control with features constraint employing Kalman-neural-network filtering scheme*, Neurocomputing **151** (2015), 268–277.
 28. X. Lv, and X. Huang, *Fuzzy adaptive Kalman filtering based estimation of image Jacobian for uncalibrated visual servoing*, IEEE International Conference on Intelligent Robots and Systems, IEEE, (2006), 2167–2172. <https://doi.org/10.1109/IROS.2006.282555>
 29. X. Ren, H. Li, and Y. Li, *Online image Jacobian identification using optimal adaptive robust Kalman filter for uncalibrated visual servoing*, 2017 2nd Asia-Pacific Conference on Intelligent Robot Systems, ACIRS 2017, IEEE (2017), 53–57. <https://doi.org/10.1109/ACIRS.2017.7986064>
 30. Y. Huang, Y. Zhang, Z. Wu, N. Li, and J. Chambers, *A novel adaptive Kalman filter with inaccurate process and measurement noise covariance matrices*, IEEE Trans. Autom. Control **63** (2018), 594–601. <https://doi.org/10.1109/TAC.2017.2730480>
 31. X. Shenshu and Z. Zhaoying, *Neural filtering of colored noise based on Kalman filter structure*, IEEE Trans. Instrum. Meas. **3** (2003), no. 52, 742–747.
 32. V. Vaidehi, N. Chitra, M. Chokkalingam, and C. N. Krishnan, *Neural network aided Kalman filtering for multitarget tracking applications*, Comput. Electr. Eng. **27** (2001), 217–228.
 33. K. Takaba, Y. Iiguni, and H. Tokumaru, *An improved tracking Kalman filter using a multilayered neural network*, Math. Comput. Model. **23** (1996), 119–128.
 34. S. A. Gadsden and S. R. Habibi, *A new robust filtering strategy for linear systems*, J. Dyn. Syst. Meas. Control Trans. ASME **135** (2013), 014503-1. <https://doi.org/10.1115/1.4006628>
 35. S. A. Gadsden, S. Habibi, and T. Kirubarajan, *Kalman and smooth variable structure filters for robust estimation*, IEEE Trans. Aerosp. Electron. Syst. **50** (2014), 1038–1050.
 36. D. Xu, J. Lu, P. Wang, Z. Zhang, and Z. Liang, *Partially decoupled image-based visual servoing using different sensitive features*, IEEE Trans. Syst. Man Cybern. Syst. **47** (2017), 2233–2243. <https://doi.org/10.1109/TSMC.2016.2641951>
 37. X. Jin, S. Wang, J. Qin, W. X. Zheng, and Y. Kang, *Adaptive fault-tolerant consensus for a class of uncertain nonlinear second-order multi-agent systems with circuit implementation*, IEEE Trans. Circuits Syst. I Regul. Pap. **65** (2018), no. 7, 2243–2255.
 38. H. Wang, L. Shi, Z. Man, J. Zheng, S. Li, M. Yu, C. Jiang, H. Kong, and Z. Cao, *Continuous fast nonsingular terminal sliding mode control of automotive electronic throttle systems using finite-time exact observer*, IEEE Trans. Ind. Electron. **65** (2018), 7160–7172.
 39. H. Shi, X. Li, K. S. Hwang, W. Pan, and G. Xu, *Decoupled visual servoing with fuzzy Q-learning*, IEEE Trans. Ind. Electron. **14** (2018), 241–252.
 40. M. Kang, H. Chen, and J. Dong, *Adaptive visual servoing with an uncalibrated camera using extreme learning machine and Q-learning*, Neurocomputing **402** (2020), 384–394.
 41. T. Poggio and F. Girosi, *A theory of networks for approximation and learning*, A.I.Memo **1140** (1989), no. 9, 1481–1497.
 42. J. Moody and C. J. Darken, *Fast learning in networks of locally-tuned processing units*, Neural Comput. **1** (1989), 281–294. <https://doi.org/10.1162/neco.1989.1.2.281>
 43. J. C. H. Watkins, *Technical note: Q-learning*, Mach. Learn. **8** (1992), 279–292.
 44. Z. Wen, Y. Wang, J. Luo, A. Kuijper, N. Di, and M. Jin, *Robust, fast and accurate vision-based localization of a cooperative target used for space robotic arm*, Acta Astronaut. **136** (2017), 101–114.

AUTHOR BIOGRAPHIES



Jinlin Gu received his BE degree in Northeastern University, Qinhuangdao, China, 2016. He is currently pursuing his PhD degree in University of Chinese Academy of Sciences and Changchun Institute of Optics, Fine Mechanics and Physics, Chinese Academy of Sciences. His current research interests include redundant robot control and robot visual servo.



Wenrui Wang received his BE degree in Jilin University, Changchun, China, 2016. He is currently pursuing his PhD degree in University of Chinese Academy of Sciences and Changchun Institute of Optics, Fine Mechanics and Physics, Chinese Academy of Sciences.



Ang Li received his BE degree in Dalian University of Technology, Dalian, China, 2010. He is currently pursuing his PhD degree in University of Chinese Academy of Sciences and Changchun Institute of Optics, Fine Mechanics and Physics, Chinese Academy of Sciences.



Mingchao Zhu received his BE and PhD degrees in Jilin University, Changchun, China, in 2003 and 2009, respectively. Since 2011, he has been an Associate Researcher in Changchun Institute of Optics, Fine Mechanics and Physics, Chinese Academy of Sciences. He is currently engaged in the Space Robotics Engineering Center and his research interests include kinematics, dynamics and control of robot.



Lihua Cao received his BE degree in Xi'an Jiaotong University, Xi'an, China, 1994. He received his PhD degree in Changchun University of Science and Technology, Changchun, China, 2014. He is currently a Researcher in Changchun Institute of Optics, Fine Mechanics and Physics, Chinese Academy of Sciences.



Zhenbang Xu received his BE and PhD degrees in University of Science and Technology of China in 2005 and 2010, respectively. From 2012 to 2017, he was an Associate Researcher in Changchun Institute of Optics, Fine Mechanics and Physics, Chinese Academy of Sciences, where he has been a Researcher since 2017. He is currently engaged as an Associate Director in the Space Robotics Engineering Center.

How to cite this article: J. Gu, W. Wang, A. Li, M. Zhu, L. Cao, and Z. Xu, *Homography-based uncalibrated visual servoing with neural-network-assisted robust filtering scheme and adaptive servo gain*, *Asian J Control* **24** (2022), 3434–3455. <https://doi.org/10.1002/asjc.2769>